



■ INFECTION

Segmental induction heating of orthopaedic metal implants

**B. G. Pijls,
I. M. J. G. Sanders,
E. J. Kuijper,
R. G. H. H. Nelissen**

Leiden University
Medical Center,
Leiden, The
Netherlands

Objectives

Prosthetic joint infection (PJI) is a devastating complication following total joint arthroplasty. Non-contact induction heating of metal implants is a new and emerging treatment for PJI. However, there may be concerns for potential tissue necrosis. It is thought that segmental induction heating can be used to control the thermal dose and to limit collateral thermal injury to the bone and surrounding tissues. The purpose of this study was to determine the thermal dose, for commonly used metal implants in orthopaedic surgery, at various distances from the heating centre (HC).

Methods

Commonly used metal orthopaedic implants (hip stem, intramedullary nail, and locking compression plate (LCP)) were heated segmentally using an induction heater. The thermal dose was expressed in cumulative equivalent minutes at 43°C (CEM43) and measured with a thermal camera at several different distances from the HC. A value of 16 CEM43 was used as the threshold for thermal damage in bone.

Results

Despite high thermal doses at the HC (7161 CEM43 to 66 640 CEM43), the thermal dose at various distances from the HC was lower than 16 CEM43 for the hip stem and nail. For the fracture plate without corresponding metal screws, doses higher than 16 CEM43 were measured up to 5 mm from the HC.

Conclusion

Segmental induction heating concentrates the thermal dose at the targeted metal implant areas and minimizes collateral thermal injury by using the non-heated metal as a heat sink. Implant type and geometry are important factors to consider, as they influence dissipation of heat and associated collateral thermal injury.

Cite this article: *Bone Joint Res* 2018;7:609–619.

Keywords: Induction heating, Periprosthetic infection, Total joint arthroplasty, Hyperthermia, Antibiotics

- B. G. Pijls, MD, PhD, Orthopaedic Surgeon, Epidemiologist,
- R. G. H. H. Nelissen, MD, PhD, Professor of Orthopaedics, Department of Orthopaedics, Leiden University Medical Center, Leiden, The Netherlands.
- I. M. J. G. Sanders, BAsC, Laboratory Technician,
- E. J. Kuijper, MD, PhD, Professor of Experimental Bacteriology, Department of Medical Microbiology, Section Experimental Bacteriology, Leiden University Medical Center, Leiden, The Netherlands.

Correspondence should be sent to B. G. Pijls; email: b.g.c.w.pijls@lumc.nl

doi: 10.1302/2046-3758.711.
BJR-2018-0080.R1

Bone Joint Res 2018;7:609–619.

Article focus

- Non-contact induction heating of metal implants is a new and emerging treatment for prosthetic joint infection (PJI). However, there is a risk of tissue necrosis with current induction heating delivery systems.
- This study investigated whether segmental induction heating can be used to control the thermal dose and to limit collateral thermal injury.
- Infrared imaging was used to estimate the thermal dose for different metal implants (hip stem, intramedullary nail, and locking compression plate (LCP)) at

various distances from the heating centre (HC).

Key messages

- Implant type and geometry are important factors to consider as they influence dissipation of heat and associated collateral thermal injury.
- For the hip stem and nail, the thermal dose was below the threshold of thermal damage beyond the HC.
- For the LCP, doses higher than the threshold were measured up to 5 mm from the HC and were lower than the threshold beyond 5 mm.

Strengths and limitations

- Segmental induction minimizes thermal dose to the adjacent metal and unexposed tissues by using the non-heated metal as a heat sink and by concentrating the thermal dose at the targeted metal implant areas.
- The heating curves of commonly used orthopaedic implants have been characterized.
- During the experiments, the heated implant was surrounded by air, not by human tissue or materials that mimic human tissue, which possibly led to an overestimation of the thermal doses.

Introduction

Prosthetic joint infection (PJI) is a devastating complication following total joint arthroplasty. It is therefore vital that new treatments for the prevention and treatment of biofilm infections in orthopaedic implants are developed.

Patients with infected implants often require multiple procedures and prolonged antibiotic therapy.¹⁻³ However, this treatment can be invasive and therefore may be impossible in patients with high comorbidity factors. Furthermore, increasing antibiotic resistance of bacteria limits the choice of antibiotics,⁴⁻⁶ and recently there have been reports that long term treatment of antibiotics for PJI actually induce antibiotic resistance.^{7,8}

A new and emerging method of treatment of PJI is non-contact induction heating (NCIH) of metal implants, and several studies have shown its effectiveness in reducing the bacterial load *in vitro* within a clinically feasible temperature range and heating duration.⁹⁻¹² NCIH of metal implants causes thermal damage to the bacterial biofilm, thereby killing the bacteria on the metal implant.⁹⁻¹² Furthermore, the heat from induction works synergistically with antibiotics to eradicate the biofilm on the metal implants.¹¹ NCIH uses pulsed electromagnetic fields (PEMF) to induce eddy currents within metallic objects.¹³ These eddy currents are electrical currents within the metallic object that oppose the change in PEMF as derived from Faraday's law of electromagnetic induction, and consequently cause heating of the metallic implant.¹³

In theory, every metal implant is suitable for induction heating, depending on its anatomical situation. The major advantage of induction heating of metallic implants is that only the metallic implant is actively heated and induction heating has no direct heating effect on the surrounding tissue. This results in the heat generated being directed onto the bacterial biofilm that is on the metal implant. The surrounding tissue, however, is heated to some extent by thermal conduction from the heated metal, but if the tissue is well perfused by blood, the heat will be significantly reduced in the same way as in blood coagulation.^{14,15}

Metal implants used for *in vitro* studies are heated entirely.⁹⁻¹² However, heating the metal implant in its

entirety *in vivo* may have disadvantages, as metal implants can have complex geometrical shapes and are also fixed to bone. These disadvantages include tissue necrosis from a high thermal dose, heterogeneous heating, and possibly loss of bone fixation.^{9-13,16-18}

Heating the metal implant by overlapping segments, segmental induction heating, has the advantage of using the non-heated metal as a heat sink, thereby theoretically minimizing the thermal dose and thermal damage to soft tissue and bone. Also, segmental induction heating allows for more homogeneous heating of a metal implant. This is particularly relevant for objects with an irregular shape such as the femoral stem of a total hip prosthesis. Homogeneous heating is important to prevent overheating of certain areas of the implant while other areas are underheated. In addition, segmental induction heating can be used for selective heating of one or two segments. For example, in the event of a more local infection, such as after intramedullary nailing for an open tibial fracture, only one or two segments of the nail may require heating. Also, areas of bone fixation can be avoided or heated to a lower temperature using segmental induction heating.

The aim of this study is to determine the thermal dose at the metal implant at several different distances from the heating centre (HC) for commonly used orthopaedic implants of different geometrical shapes. The hypothesis is that segmental induction heating can be used for selective heating, thus concentrating the thermal dose and at the same time minimizing the thermal dose to the adjacent metal and tissues not being treated.

Materials and Methods

Heating of metal implants was performed using a custom-built induction heater that produced a PEMF of 360 kHz and 135 W. The induction heater featured a 13-turn solenoid heating coil with an inner diameter of 24 mm in a modified Helmholtz configuration: two connected 6.5-turn solenoid coils (totals 13) with 12 mm spacing between them. The metal implant was placed in the 12 mm space perpendicular to the solenoid, allowing segmental non-contact heating. The coil was positioned parallel to the table with the opening of the solenoid coil facing the infrared thermal camera in such a way that the camera could look through the coil in order to visualize the part of the implant that was being heated. Figure 1 and the Supplementary Material show the setup of the experiment.

The following commonly used implants were investigated: 1) hip stem (Corail, size 11; DePuy Synthes, Warsaw, Indiana), hydroxyapatite-coated titanium alloy (Ti6Al4V); 2) intramedullary nail (Y-nail, 420 mm long, 11 mm diameter; Stryker, Kalamazoo, Michigan), titanium alloy (Ti6Al4V); and 3) locking compression plate (LCP) (16 holes, stainless steel; DePuy Synthes).

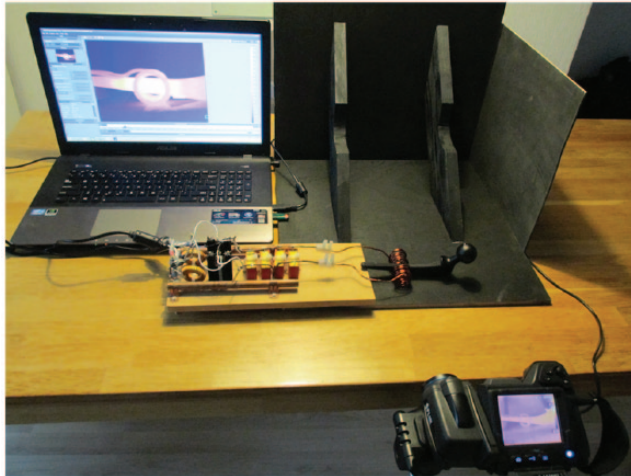


Fig. 1

A photograph showing experimental setup for thermal measurements during segmental induction heating of metal implant, in this case the hip stem.

The target temperature was 60°C , which was chosen as this has been previously shown to be effective at inactivating planktonic bacteria and potentiating antibiotic activity against biofilm-associated organisms.^{10,11}

The *in vivo* temperature of the implant is similar to core body temperature (37°C), requiring an additional 23°C to achieve the target bactericidal temperature of 60°C . Therefore, the temperature increase of interest in this investigation was 23°C above room temperature, which was approximately 20°C .^{10,16} From this, the thermal dose was estimated to be 43°C , and was expressed in cumulative equivalent minutes (CEM43).^{10,16}

Thermal imaging. Thermal imaging was performed with an infrared thermal camera (T440 thermal imaging infrared camera; FLIR Systems Inc., Wilsonville, Oregon) with a resolution of 320×240 pixels. Thermal imaging was used as it can demonstrate the heat distribution on the surface of the metal implant while simultaneously allowing multiple spot thermal measurements to be taken. In infrared thermal imaging, the measured temperature is affected by emissivity of a surface. Emissivity of an object is the ratio of the amount of radiation actually emitted from the surface to that emitted by a blackbody at the same temperature.¹⁹ Some materials are more emissive than others. For instance, glossy or reflective materials like metals tend to have a low emissivity, meaning that the measured temperature with infrared imaging is lower than the actual temperature of the surface of the object.¹⁹ To allow for accurate thermal measurements, we adjusted the emissivity of the metal implants by coating them with a thin layer of matte black paint (Fig. 2).¹⁹ A K-type thermocouple was used in order to compare the temperatures of the matte-coated metal implant, measured using the thermal camera, with the thermocouple after the PEMF had been switched off. This was because PEMF may affect the thermocouple's measurements.



Fig. 2a

Fig. 2b

a) Photograph showing the hip stem with a thin layer of black paint and without coating. b) Thermal image of hip stem with and without coating. The emissivity of coated stem is improved, allowing uniform and accurate temperature measurements.

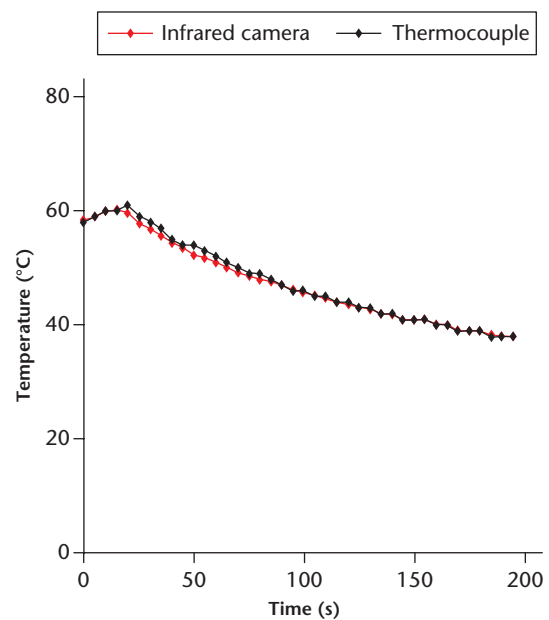


Fig. 3

Graph depicting temperature measurements of a hip stem after induction heating with thermal camera (infrared camera) and K-type thermocouple. The measurements are nearly identical.

Thermal dose calculation. The thermal dose CEM43 is a widely used metric that converts all thermal exposures to 'equivalent-minutes' at 43°C , allowing for comparison of the thermal doses of different temperatures and duration.²⁰ The thermal dose in CEM43 at the edge/skin of the metal implant represents the thermal dose at the bone-implant interface or tissue-implant interface and hence is the dose to which the cells directly on the edge/skin of the metal implant are exposed. For bone, 16 CEM43 is an indicator of thermal damage, and for muscle, 240 CEM43 is an indicator of irreversible thermal damage.^{21,22} Therefore, 16 CEM43 and 240 CEM43 were used as the threshold values at which thermal damage could occur.^{21,22} The CEM43 thermal dose was determined in the HC and at several distances from it in a 3×3 pixel area that was directly

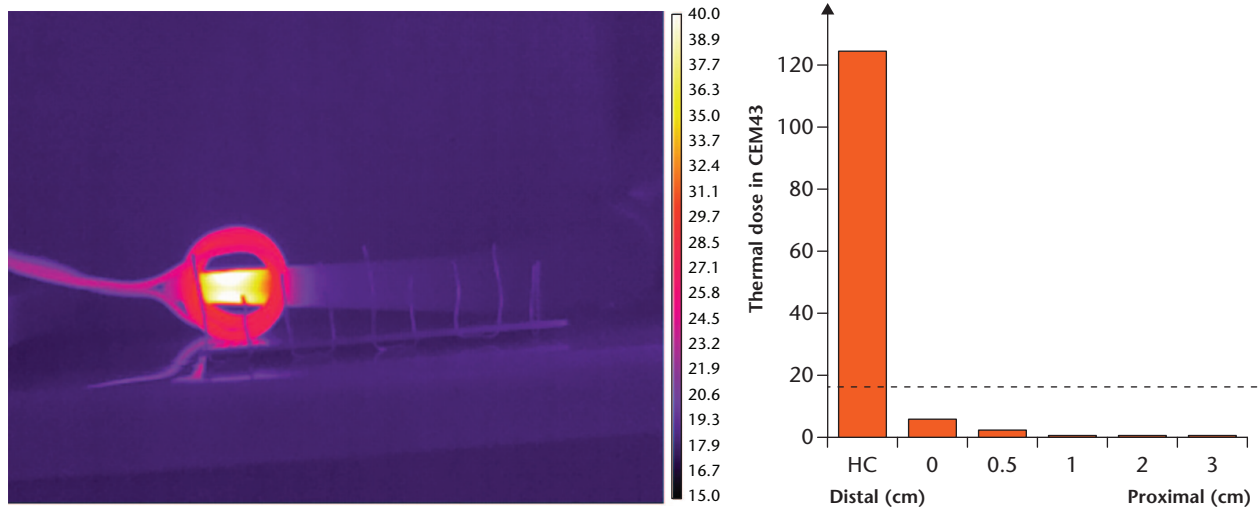


Fig. 4a

Fig. 4b

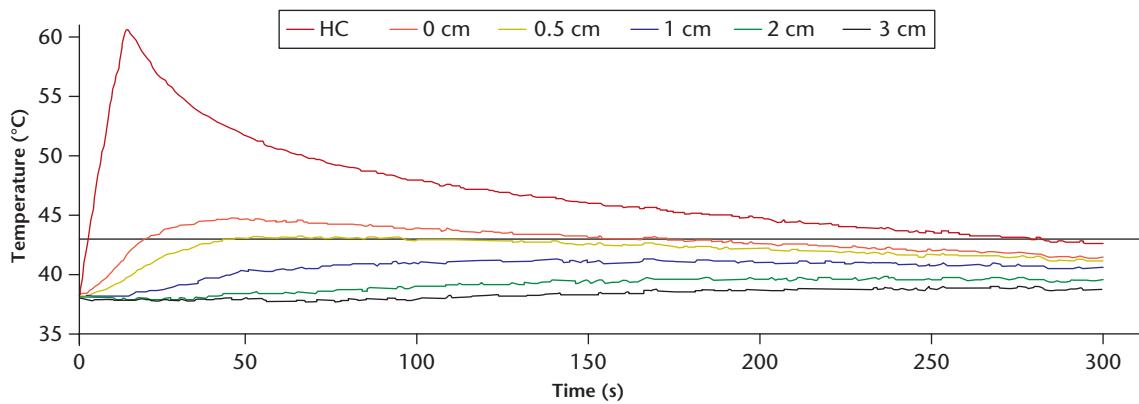


Fig. 4c

Segmental induction heating of hip stem, distally. a) A thermal image from a thermal camera showing selective heating. The vertical lines have 1 cm spacing. b) A graph showing thermal dose in CEM43 at several distances from the heating centre (HC). The dashed line represents 16 CEM43, the threshold for necrosis of bone. c) A graph showing the temperature at several distances from the HC during the segmental induction heating and thereafter.

adjacent to the coil (0 cm from coil), as well as at 0.5 cm, 1.0 cm, 2.0 cm, and 3.0 cm from the coil. Temperatures were recorded at these distances every second.

The femoral stem was heated at the proximal end, at the distal end, and in the centre of the stem because it is tapered and non-symmetrical. The intramedullary nail was heated in the centre because it is mostly symmetrical in the proximal and distal direction.

Since the LCP has different geometry at the front and underside of the plate, the thermal dose was determined for the front and underside separately while it was heated in the centre. The heating cycle and imaging was performed once for every implant and position.

Statistical analysis. The following formula is applied to calculate CEM43:²⁰

$$CEM43 = \int_0^t r^{43-T}, r = \begin{cases} 0.25, & T < 43 \\ 0.50, & T \geq 43 \end{cases}$$

The calculated thermal dose expressed in units of CEM43 was subsequently compared with the thresholds of 16 CEM43 for bone and 240 CEM43 for muscle to determine if the thermal dose would lead to tissue necrosis.^{21,22}

Intraclass correlation (ICC) was used to compare the temperature measured with the thermal camera with the temperature measured by the K-type thermocouple. Linear regression was employed to calculate the association between 'time to reach target temperature' and the thermal dose at 0 cm and 0.5 cm while correcting for distance with 95% confidence intervals (CIs). Descriptive statistics were used when appropriate.

Results

The temperature measurements of the thermal camera and K-type thermocouple are depicted in Figure 3. The ICC of the temperatures measured with the thermal

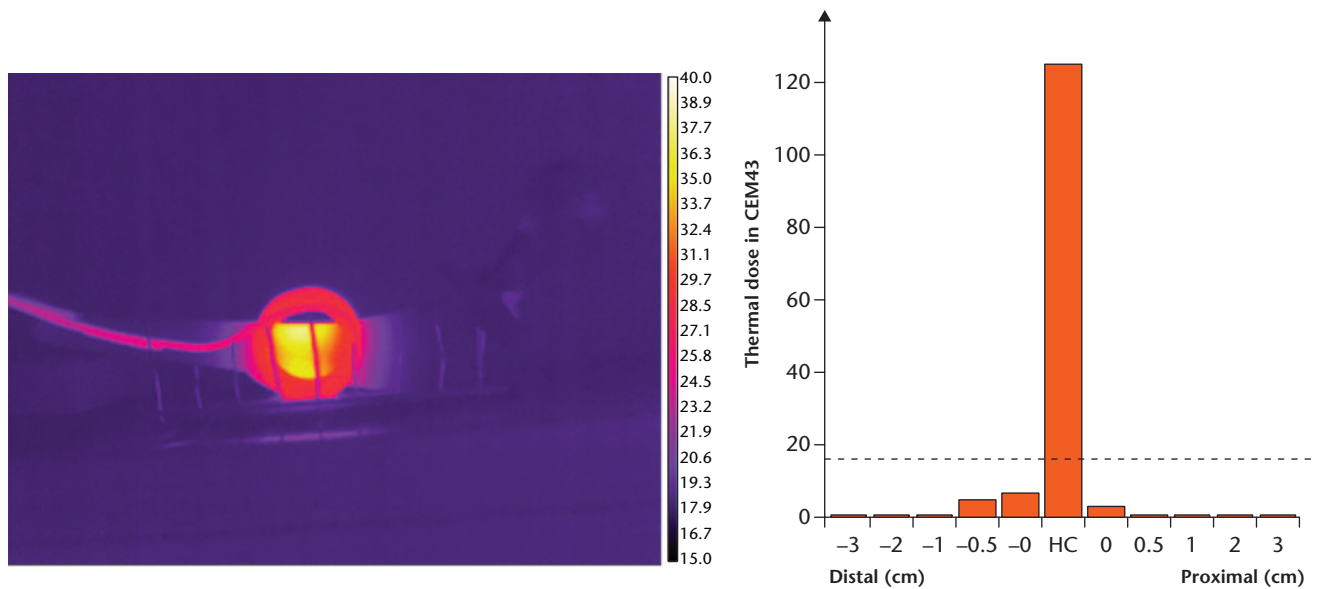


Fig. 5a

Fig. 5b

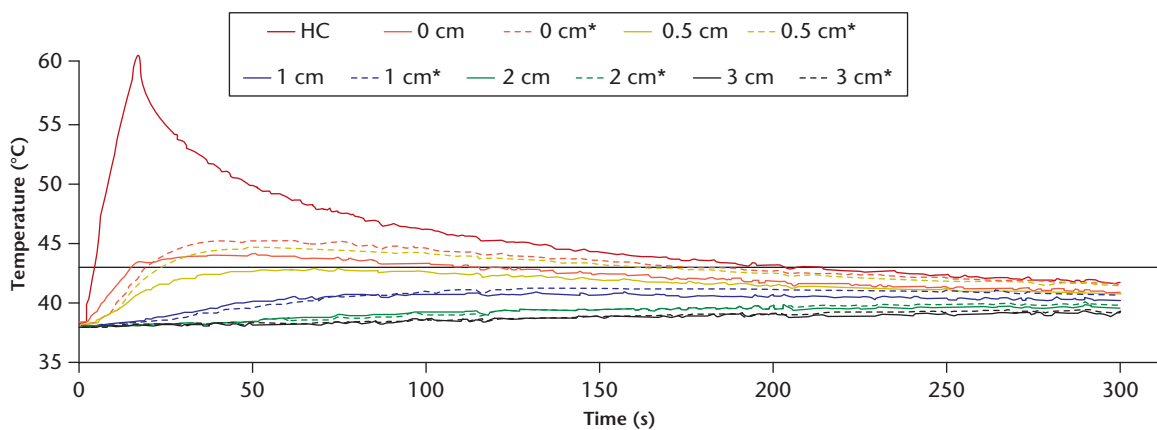


Fig. 5c

Segmental induction heating of hip stem centre. a) A thermal image from a thermal camera showing selective heating. The vertical lines have 1 cm spacing. b) A graph showing thermal dose in CEM43 at several distances from the heating centre (HC). The dashed line represents 16 CEM43, the threshold for necrosis of bone. c) A graph showing the temperature at several distances from the HC during the segmental induction heating and thereafter. Dashed lines indicate distal direction.

camera and K-type thermocouple is 0.99 (95% CI 0.99 to 1.00), indicating near-perfect agreement.

Hip stem. Heating of the distal end of the hip stem took 13 seconds to reach the target temperature, accumulating a thermal dose of 17 385 CEM43 at the HC. The temperature profile as well as the thermal dose at several distances from the heating coil are depicted in Figure 4. For all distances from the heating coil, the CEM43 was below 16 CEM43.

Heating of the centre of the hip stem took 14 seconds to reach the target temperature, accumulating a thermal dose of 71 611 CEM43 at the HC. The temperature profile as well as the thermal dose at several distances from the heating coil are depicted in Figure 5. For all distances from the heating coil, the CEM43 was below 16 CEM43. The distal part, which has a smaller taper and less metal

to act as heat sink, seemed to have a slightly higher thermal dose than the proximal part.

Heating of the proximal end of the hip stem took 23 seconds to reach the target temperature, accumulating a thermal dose of 66 640 CEM43 at the HC. The temperature profile, as well as the thermal dose at several distances from the heating coil, is depicted in Figure 6. For 0 cm distal to the heating coil, the thermal dose was 16.8 CEM43, which is more than the 16 CEM43 threshold. For all other distances from the heating coil, the CEM43 was below 16 CEM43. The distal part, with the smaller taper and less metal to act as heat sink, seemed to have a higher thermal dose than the proximal part.

Intramedullary nail. Heating of the intramedullary nail took 12 seconds to reach the target temperature, accumulating a thermal dose of 14 418 CEM43 at the HC. The

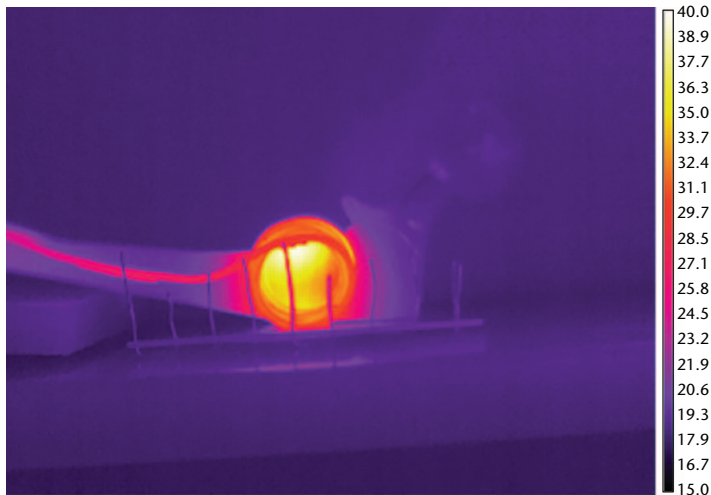


Fig. 6a

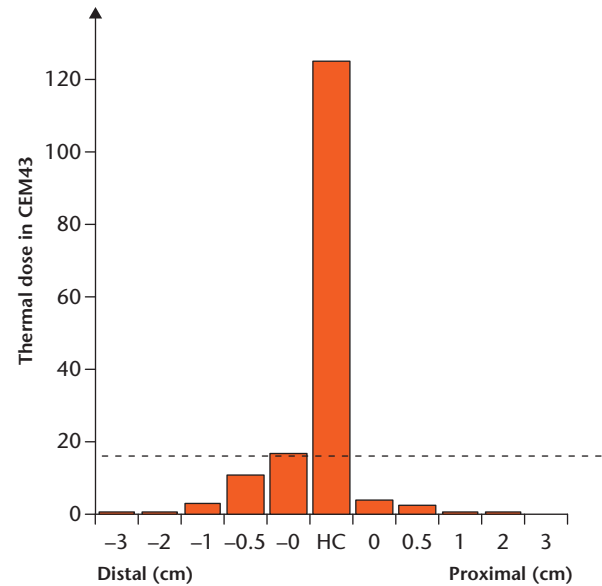


Fig. 6b

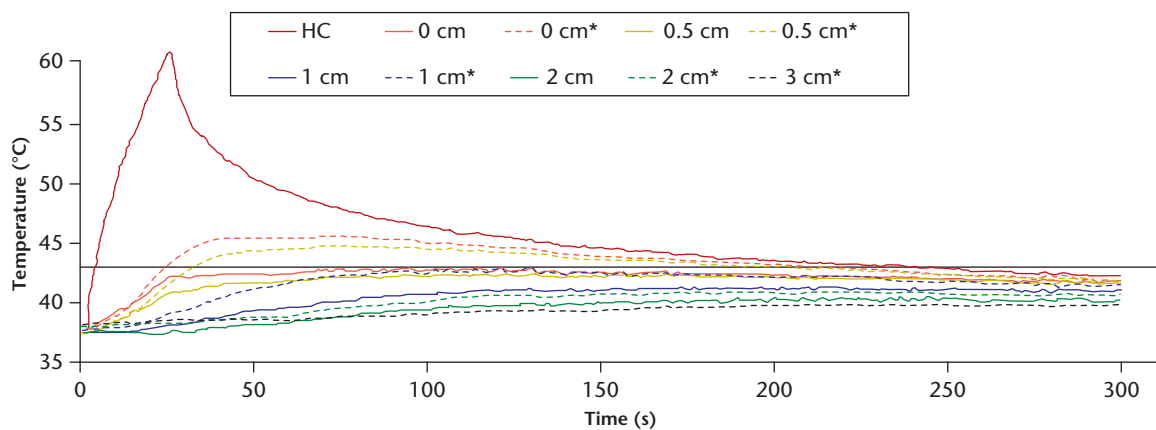


Fig. 6c

Segmental induction heating of hip stem, proximally. a) A thermal image from a thermal camera showing selective heating. The vertical lines have 1 cm spacing. b) A graph showing thermal dose in CEM43 at several distances from the heating centre (HC). The dashed line represents 16 CEM43, the threshold for necrosis of bone. c) A graph showing the temperature at several distances from the HC during the segmental induction heating and thereafter. Dashed lines indicate distal direction.

temperature profile, as well as the thermal dose at several distances from the heating coil, is depicted in Figure 7. For all distances from the heating coil, the CEM43 was below 16 CEM43.

Locking compression plate (LCP). From the front, heating of the LCP took 57 seconds to reach the target temperature, accumulating a thermal dose of 31 860 CEM43 at the HC. The temperature profile as well as the thermal dose at several distances from the heating coil are depicted in Figure 8. For 0 cm distal and proximal to the heating coil, the thermal dose was 32.6 CEM43 and 16.1 CEM43, respectively, and for 0.5 cm distal to the heating coil the thermal dose was 16.4 CEM43, which is more than the 16 CEM43 threshold. For all other distances from the heating coil, the CEM43 was below 16 CEM43.

The location of holes seemed to affect the thermal dose and the thermal doses seemed to be higher distally.

From the underside of the LCP, heating took 54 seconds to reach the target temperature, accumulating a thermal dose of 20974 CEM43 at the HC. The temperature profile, as well as the thermal dose at several distances from the heating coil, is depicted in Figure 9. For 0 cm distal and proximal to the heating coil, the thermal dose was 110 CEM43 and 36.6 CEM43, respectively, and for 0.5 cm distal and proximal to the heating coil the thermal dose was 53.1 CEM43 and 16.49 CEM43, respectively, which is more than the 16 CEM43 threshold. For all other distances from the heating coil, the CEM43 was below 16 CEM43. The location of holes seemed to affect the thermal dose, with the thermal doses being higher distally.

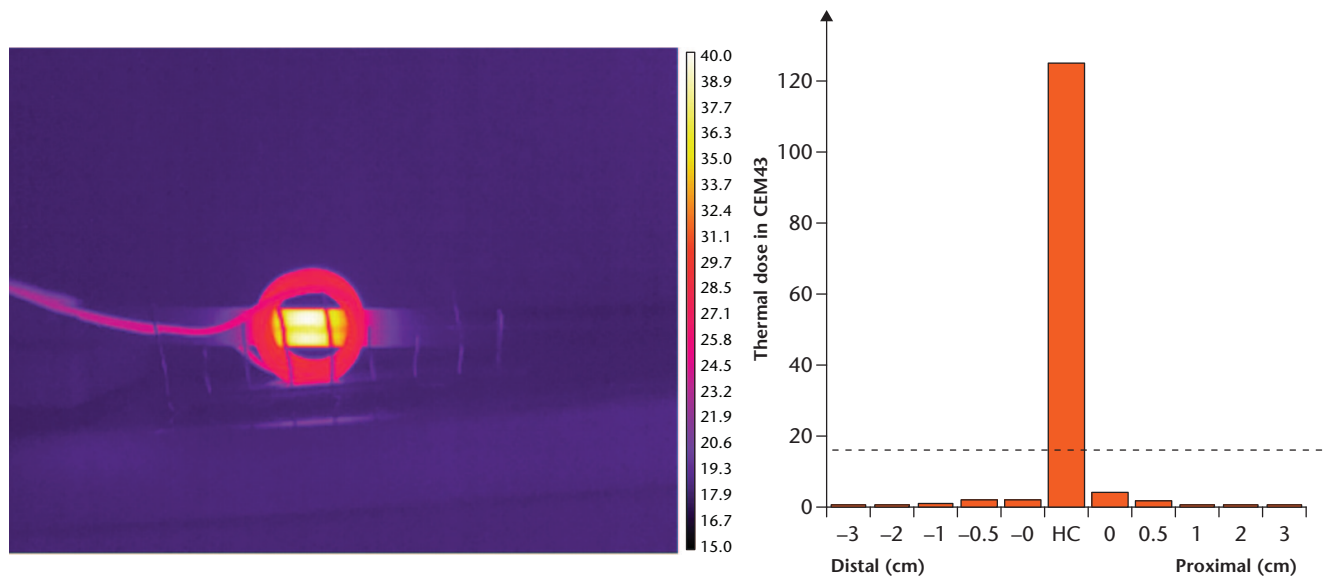


Fig. 7a

Fig. 7b

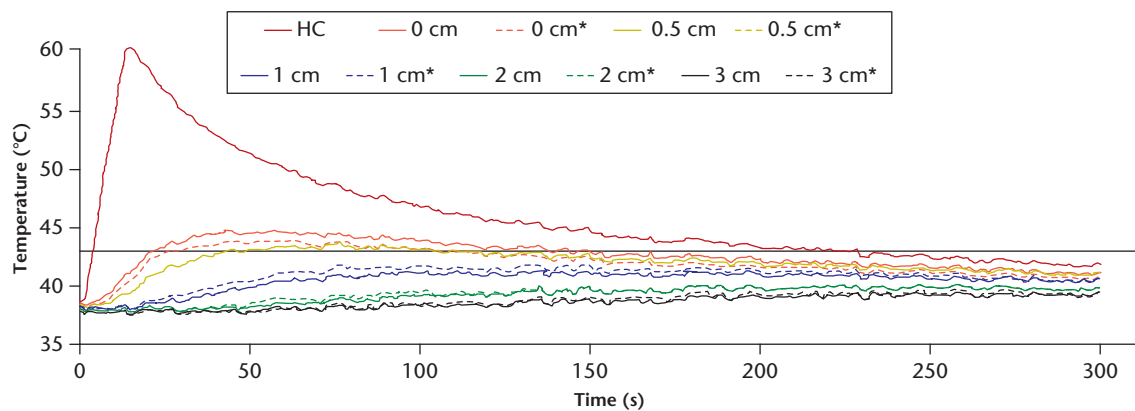


Fig. 7c

Segmental induction heating of intramedullary (IM) nail. a) A thermal image from a thermal camera showing selective heating. The vertical lines have 1 cm spacing. b) A graph showing thermal dose in CEM43 at several distances from the heating centre (HC). The dashed line represents 16 CEM43, the threshold for necrosis of bone. c) A graph showing the temperature at several distances from the HC during the segmental induction heating and thereafter. Dashed lines indicate distal direction.

We found that there was a significant association between the time to reach the target temperature and the thermal dose for 0 cm (directly next to the heating coil and the coil is not touching the implant) and 0.5 cm distance from the heating coil. For every second of increased time to reach the target temperature, 0.77 CEM43 (95% CI 0.31 to 1.22) was added to the thermal dose (linear regression; $p = 0.002$).

Discussion

The results of our study show that segmental induction heating can be used to heat selectively a segment of a metal orthopaedic implant using the non-heated part of the implant as a heat sink. Despite high thermal doses at the HC (7161 CEM43 to 66640 CEM43), the thermal dose at several distances from the HC was generally lower

than 16 CEM43, indicating no damage occurred to the bone.^{21,22} In all cases, the thermal dose at several distances from the HC was lower than 240 CEM43, indicating no damage to the muscle.^{21,22} Hence segmental induction heating offers greater flexibility, providing homogeneous heating and allowing for a tailored solution compared with heating the entire implant at once.

The heating profile for the implants used in our study is similar to the heating profiles from other groups where there were high thermal doses (7161 CEM43 to 66640 CEM43) at the HC compared with the thresholds of thermal damage of 16 CEM43 for bone and 240 CEM43 for muscle.^{9,17,18,23} It is of interest that animal experiments have shown little or no thermal damage to surrounding tissue due to induction heating of a metal implant using similar heating profiles. Müller et al¹⁷ heated a nickel-titanium

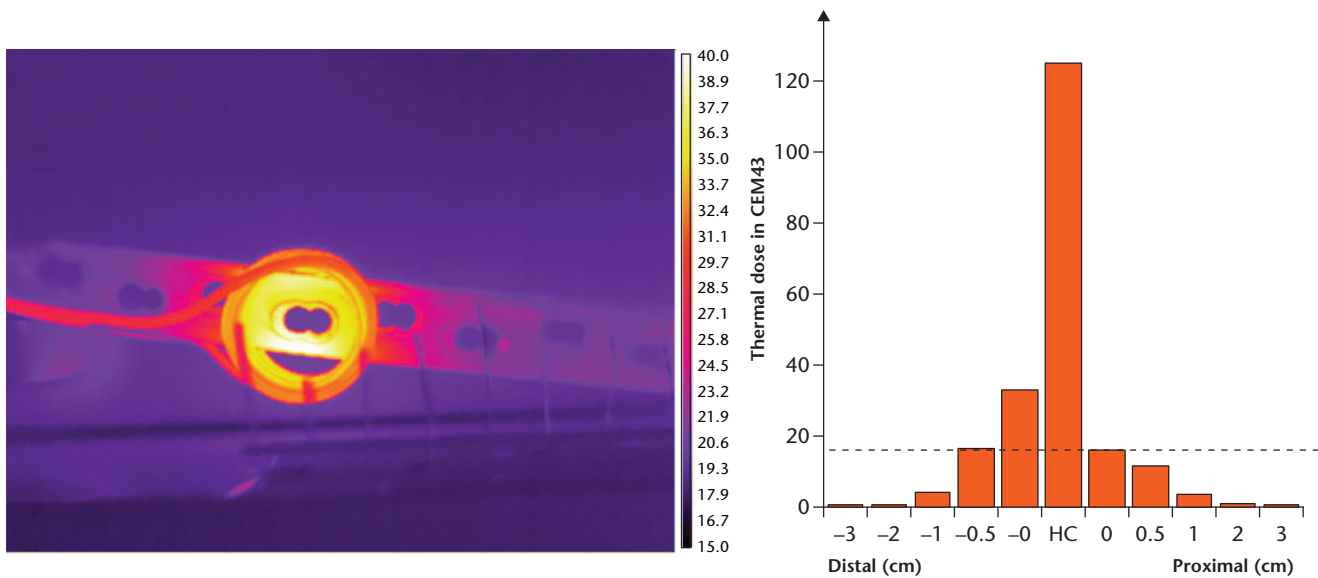


Fig. 8a

Fig. 8b

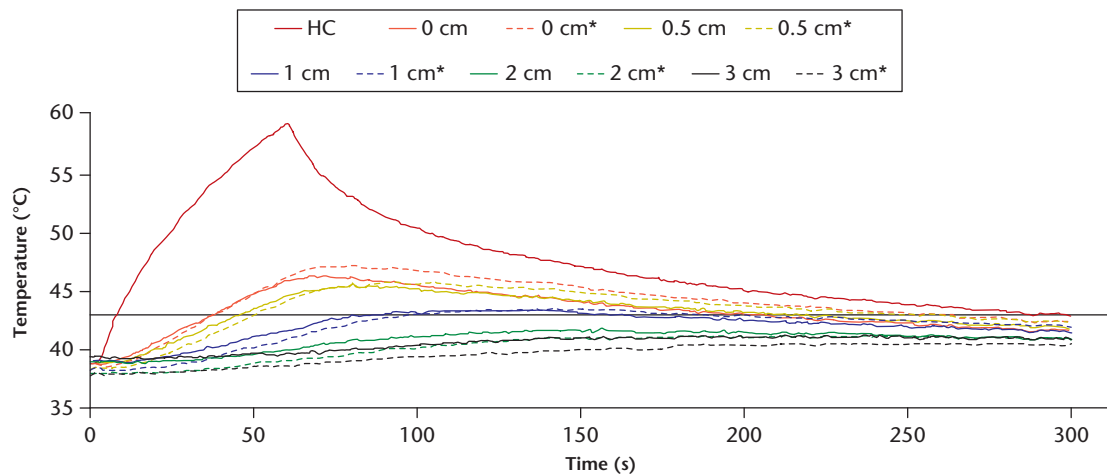


Fig. 8c

Segmental induction heating of locking compression plate (LCP), front view. a) A thermal image from a thermal camera showing selective heating. The vertical lines have 1 cm spacing. b) A graph showing thermal dose in CEM43 at several distances from the heating centre (HC). The dashed line represents 16 CEM43, the threshold for necrosis of bone. c) A graph showing the temperature at several distances from the HC during the segmental induction heating and thereafter. Dashed lines indicate distal direction.

shape memory rod in the femur of rats at 40°C to 60°C using induction heating and found no evidence of necrosis of the surrounding bone and tissues. They also heated an osteosynthesis plate in a rabbit model with induction heating and noted that all osteotomies underneath the plate healed.¹⁸ Chopra et al⁹ have shown in a mouse model that thermal damage is confined to a localized region (< 2 mm) around the implant. Fang et al¹² heated metal implants in a rat model to 75°C without any significant thermal damage on the surrounding tissue. These studies are in agreement with Samara et al,²⁴ who have shown that bone cement achieves durable fixation despite the temperature reaching 80°C for more than ten minutes, caused by the curing process of the cement.

Chopra et al⁹ and Müller et al^{17,18} have suggested that the target temperature should be achieved rapidly when heating metal implants with induction heating in order to minimize the thermal damage to surrounding tissue. The results of our study confirm and quantify those suggestions, as for every second increase in time to reach the target temperature, 0.77 CEM43 was added to the thermal dose.

The non-heated parts of the metal implant work as a heat sink. If the implant is heated in the centre and one side of the non-heated part (for example, the distal part, which has a decreasing cross-sectional area) compared with the other non-heated part (for example, the proximal part, which has an increasing cross-sectional area), it was found that the part with the decreasing cross-sectional

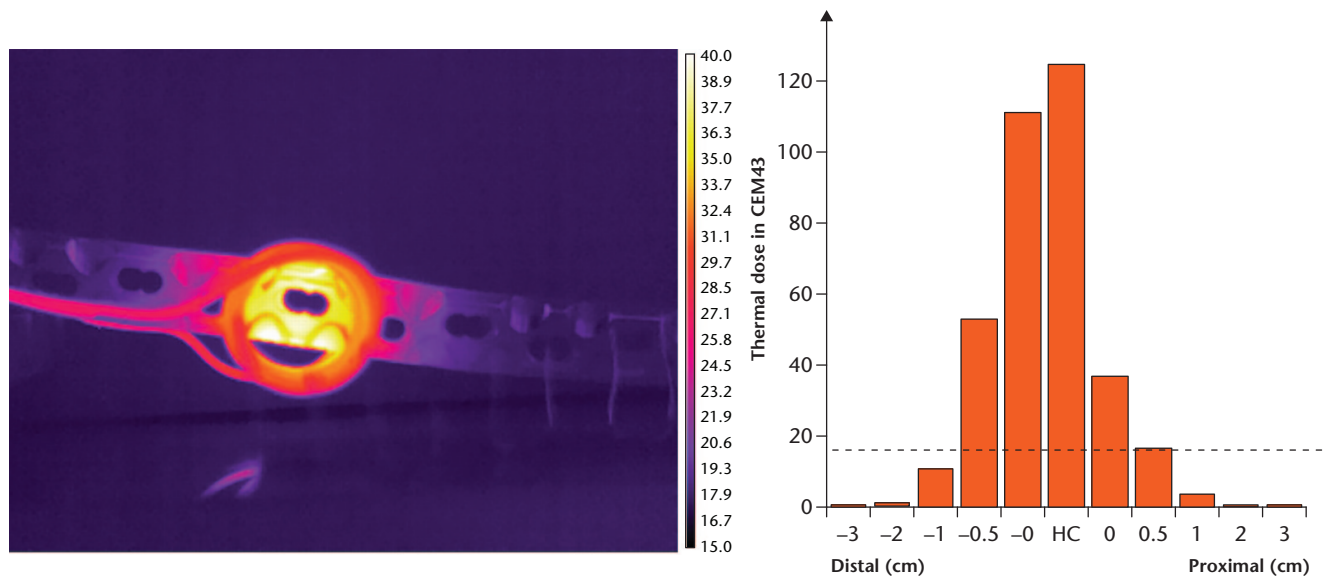


Fig. 9a

Fig. 9b

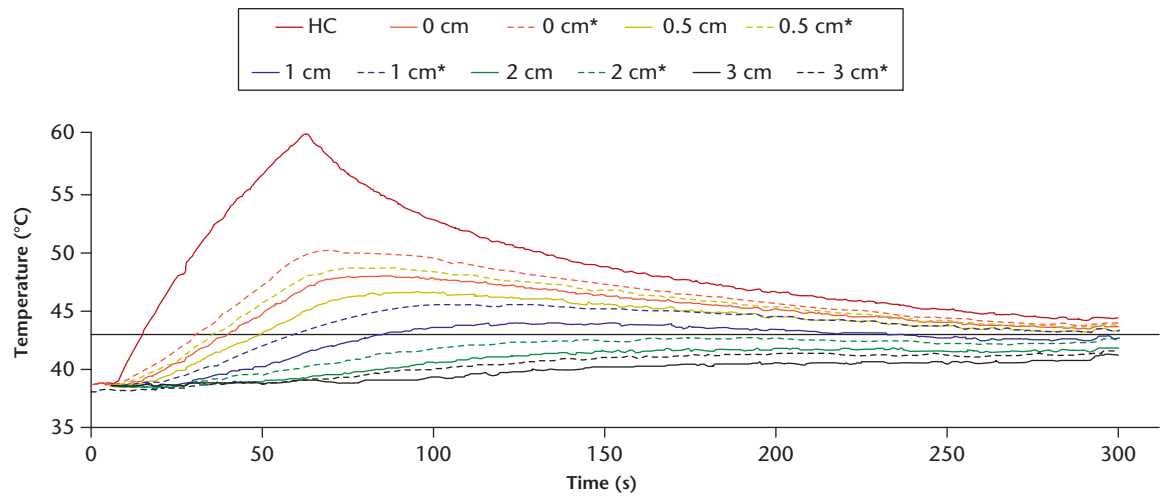


Fig. 9c

Segmental induction heating of locking compression plate (LCP), underside. a) A thermal image from a thermal camera showing selective heating. The vertical lines have 1 cm spacing. b) A graph showing thermal dose in CEM43 at several distances from the heating centre (HC). The dashed line represents 16 CEM43, the threshold for necrosis of bone. c) A graph showing the temperature at several distances from the HC during the segmental induction heating and thereafter. Dashed lines indicate distal direction.

area reached higher temperatures, resulting in the surrounding tissues being exposed to higher thermal doses. This was observed in the tapered stem hip design (Figs 5 and 6) where the distal part had a decreasing cross-sectional area compared with the proximal part, resulting in the thermal dose being higher for the distal than the proximal part. We also observed this phenomenon in the LCP (Figs 8 and 9). The holes in the plate and the geometry of the underside, the bone side, decrease the cross-sectional area and funnel the heat, resulting in an increased thermal dose. It should be noted, however, that when the LCPs are used clinically the holes in the plate will be filled with metal screws, which in turn act as a heat sink. In contrast

to these irregularly shaped metal implants, the distribution of the thermal dose was symmetrical for a symmetrical implant such as the intramedullary nail (Fig. 7).

This study has the following limitations. During the experiments, the heated implant was surrounded by air, not by human tissue or materials that mimic human tissue. This experimental setup was necessary when using the infrared camera, which required a direct line of vision. As the thermal conductivity of air and human tissue, such as muscle or bone, are different, this will affect the interpretation of our data. The thermal conductivity of air at room temperature is $0.0257 \text{ Watt} \times \text{metre}^{-1} \times \text{Kelvin}^{-1} (\text{Wm}^{-1} \text{K}^{-1})$, the thermal conductivity of bone is $0.32 \text{ Wm}^{-1} \text{K}^{-1}$, the

thermal conductivity of blood is $0.52 \text{ Wm}^{-1} \text{ K}^{-1}$, and the thermal conductivity of muscle is $0.49 \text{ Wm}^{-1} \text{ K}^{-1}$.^{25,26} Air can therefore be considered a thermal insulator compared with bone or muscle. The heat capacity of air is $1006 \text{ Joule} \times \text{kilogram}^{-1} \times \text{Kelvin}^{-1}$ ($\text{Jkg}^{-1} \text{ K}^{-1}$), the heat capacity of bone is $1908 \text{ Jkg}^{-1} \text{ K}^{-1}$, the heat capacity of muscle is $1090 \text{ Jkg}^{-1} \text{ K}^{-1}$, and the heat capacity of blood is $1050 \text{ Jkg}^{-1} \text{ K}^{-1}$.^{25,26} Therefore, with the same amount of heat energy delivered at the HC, *in vivo*, more heat will be conducted to the bone and muscle, probably resulting in faster cooling and lower CEM43 values for the non-heated parts of the metal implant. The heating of metal implants with segmental induction heating will therefore probably be even more selective *in vivo* with lower thermal damage to the tissues surrounding the non-heated parts of the implant.

In our experiment, the distance between the metal implant and the heating coil was a few millimetres. In clinical application, however, this distance will be several centimetres or more, and the field strength of the PEMF is known to decay rapidly with distance.¹⁰ Scaling of the induction heating coil for clinical application clearly requires specialized and optimized designs,²⁷ which were not available for this investigation.

We chose 60°C as the target temperature based on studies of planktonic bacteria and bacteria within a biofilm.^{10,11} Although 60°C may or may not be the optimal temperature, it does fall within the range of effective temperatures for killing bacteria within a biofilm.⁹⁻¹¹ We also chose 60°C as it is on the lower end of the spectrum of effective temperatures, and future studies will aim at further reducing the thermal dose.^{11,28}

The required temperatures and time to kill bacteria in a biofilm range from 60°C to 90°C for one to ten minutes,⁹⁻¹¹ resulting in a high thermal dose and tissue damage. Hajdu et al²⁸ have shown that the antibacterial activity of antimicrobial agents is significantly enhanced by increasing the ambient temperature. Recently, Ricker and Nuxoll¹¹ have confirmed this synergistic effect of antibiotics and heat in a *Pseudomonas* biofilm. These findings suggest that biofilms may be eliminated at lower temperatures and lower exposure times than previously observed when combined with antibiotics.^{11,28}

In conclusion, segmental induction heating concentrates the thermal dose on focal areas of metal implants, thus minimizing collateral thermal injury by using the non-heated metal as a heat sink. Implant design and geometry are important factors to consider when induction heating is used as they influence dissipation of heat and associated collateral thermal injury.

Supplementary material

 A video showing experimental setup for thermal measurements during segmental induction heating of metal implant, in this case the hip stem.

References

1. Tande AJ, Patel R. Prosthetic joint infection. *Clin Microbiol Rev* 2014;27:302-345.
2. Tayton ER, Frampton C, Hooper GJ, Young SW. The impact of patient and surgical factors on the rate of infection after primary total knee arthroplasty: an analysis of 64,566 joints from the New Zealand Joint Registry. *Bone Joint J* 2016;98-B:334-340.
3. Jacobs AME, Bénard M, Meis JF, van Hellemond G, Goosen JHM. The unsuspected prosthetic joint infection: incidence and consequences of positive intra-operative cultures in presumed aseptic knee and hip revisions. *Bone Joint J* 2017;99-B:1482-1489.
4. Anguita-Alonso P, Hanssen AD, Osmon DR, et al. High rate of aminoglycoside resistance among staphylococci causing prosthetic joint infection. *Clin Orthop Relat Res* 2005;439:43-47.
5. Ravi S, Zhu M, Luey C, Young SW. Antibiotic resistance in early periprosthetic joint infection. *ANZ J Surg* 2015;86:1014-1018.
6. Gomes DM, Ward KE, LaPlante KL. Clinical implications of vancomycin heteroresistant and intermediately susceptible *Staphylococcus aureus*. *Pharmacotherapy* 2015;35:424-432.
7. Corona PS, Espinal L, Rodríguez-Pardo D, et al. Antibiotic susceptibility in gram-positive chronic joint arthroplasty infections: increased aminoglycoside resistance rate in patients with prior aminoglycoside-impregnated cement spacer use. *J Arthroplasty* 2014;29:1617-1621.
8. Schmolders J, Hischebeth GT, Friedrich MJ, et al. Evidence of MRSE on a gentamicin and vancomycin impregnated polymethyl-methacrylate (PMMA) bone cement spacer after two-stage exchange arthroplasty due to periprosthetic joint infection of the knee. *BMC Infect Dis* 2014;14:144.
9. Chopra R, Shaikh S, Chatzinoff Y, et al. Employing high-frequency alternating magnetic fields for the non-invasive treatment of prosthetic joint infections. *Sci Rep* 2017;7:7520.
10. Pijls BG, Sanders IMJG, Kuijper EJ, Nelissen RGHH. Non-contact electromagnetic induction heating for eradicating bacteria and yeasts on biomaterials and possible relevance to orthopaedic implant infections: *in vitro* findings. *Bone Joint Res* 2017;6:323-330.
11. Ricker EB, Nuxoll E. Synergistic effects of heat and antibiotics on *Pseudomonas aeruginosa* biofilms. *Biofouling* 2017;33:855-866.
12. Fang CH, Tsai PI, Huang SW, et al. Magnetic hyperthermia enhance the treatment efficacy of peri-implant osteomyelitis. *BMC Infect Dis* 2017;17:516.
13. Cheng DK. *Field and Wave Electromagnetics (International Edition)*. Massachusetts: Addison-Wesley Publishing Company, 1989.
14. de Berg JC, Pattynama PM, Obermann WR, et al. Percutaneous computed-tomography-guided thermocoagulation for osteoid osteomas. *Lancet* 1995;346:350-351.
15. Tillotson CL, Rosenberg AE, Rosenthal DI. Controlled thermal injury of bone. Report of a percutaneous technique using radiofrequency electrode and generator. *Invest Radiol* 1989;24:888-892.
16. Pfeifer R, Hustedt M, Wesling V, et al. Noninvasive induction implant heating: an approach for contactless altering of mechanical properties of shape memory implants. *Med Eng Phys* 2013;35:54-62.
17. Müller CW, ElKashef T, Pfeifer R, et al. Transcutaneous electromagnetic induction heating of an intramedullary nickel-titanium shape memory implant. *Int Orthop* 2014;38:2551-2557.
18. Müller CW, Pfeifer R, Meier K, et al. A novel shape memory plate osteosynthesis for noninvasive modulation of fixation stiffness in a rabbit tibia osteotomy model. *Biomed Res Int* 2015;2015:652940.
19. Vollmer M, Möllmann K-P. *Infrared Thermal Imaging. Fundamentals, Research and Applications*. Second ed. Wiley, 2010.
20. Sapareto SA, Dewey WC. Thermal dose determination in cancer therapy. *Int J Radiat Oncol Biol Phys* 1984;10:787-800.
21. van Rhoon GC, Samaras T, Yarmolenko PS, et al. CEM43°C thermal dose thresholds: a potential guide for magnetic resonance radiofrequency exposure levels? *Eur Radiol* 2013;23:2215-2227.
22. Chung AH, Jolesz FA, Hynynen K. Thermal dosimetry of a focused ultrasound beam *in vivo* by magnetic resonance imaging. *Med Phys* 1999;26:2017-2026.
23. Cheng B, Chatzinoff Y, Szczepanski D, et al. Remote acoustic sensing as a safety mechanism during exposure of metal implants to alternating magnetic fields. *PLoS One* 2018;13:e0197380.
24. Samara E, Moriarty TF, Decosterd LA, et al. Antibiotic stability over six weeks in aqueous solution at body temperature with and without heat treatment that mimics the curing of bone cement. *Bone Joint Res* 2017;6:296-306.
25. No authors listed. Air – Thermophysical Properties. *The Engineering Toolbox*. 2003. https://www.engineeringtoolbox.com/air-properties-d_156.html (date last accessed 20 July 2018).

26. **Hasgall PA, Di Gennaro F, Baumgartner C, et al.** IT'IS Database for thermal and electromagnetic parameters of biological tissues. Version 4.0, 2018. www.itis.ethz.ch/database (date last accessed 20 July 2018).
27. **Huang CF, Chao HY, Chang HH, Lin XZ.** A magnetic induction heating system with multi-cascaded coils and adjustable magnetic circuit for hyperthermia. *Electromagn Biol Med* 2016;35:59-64.
28. **Hajdu S, Holinka J, Reichmann S, et al.** Increased temperature enhances the antimicrobial effects of daptomycin, vancomycin, tigecycline, fosfomycin, and cefamandole on staphylococcal biofilms. *Antimicrob Agents Chemother* 2010; 54:4078-4084.

Funding Statement

- This research has been funded by ZonMw "off road" grant 451001003.

Acknowledgements

- We would like to thank FLIR Systems inc, in particular Ruud Heijnsman and Koen Jacobs, for providing thermal imaging equipment and help with the experimental setup.

Author Contributions

- B. G. Pijls: Designed the study, Performed the experiments, Analyzed the data, Wrote and critically revised the manuscript.
- I. M. J. G. Sanders: Designed the study, Wrote and critically revised the manuscript.
- E. J. Kuijper: Designed the study, Critically revised the manuscript.
- R. G. H. H. Nelissen: Designed the study, Wrote and critically revised the manuscript.

Conflict of Interest Statement

- None declared

© 2018 **Author(s) et al.** This is an open-access article distributed under the terms of the Creative Commons Attribution licence (CC-BY-NC), which permits unrestricted use, distribution, and reproduction in any medium, but not for commercial gain, provided the original author and source are credited.